ELSEVIER

S0032-3861(96)00637-4

Polymer Vol. 38 No. 5, pp. 1091–1100, 1997

0032-3861/97/$17.00 + 0.00

High performance PET fibre properties achieved at high speed using a combination of threadline modification and traditional post treatment

Gang Wu*, Paul A. Tucker and John A. Cuculo
Fibre and Polymer Science Program, College of Textiles, North Carolina State University, Raleigh, NC 27695-8301, USA
(Received 2 June 1994)

A process was investigated for producing high modulus, high strength, dimensionally stable poly(ethylene terephthalate) (PET) filament by combination of threadline modification and post drawing techniques. Unlike traditional commercial processes for the production of PET filament yarn, the present process uses a liquid isothermal bath to develop an extremely high level of tension in the threadline. This results in extremely high amorphous orientation and low crystallinity in the as-spun fibres, with good mechanical properties, similar to those found in products produced using a commercial spin–draw process. The oriented amorphous structure produced directly by such a modified spinning process can be further oriented by a subsequent hot-drawing operation, resulting in a final PET filament product which possesses ultra-high birefringence ($\Delta n > 0.23$) and excellent mechanical properties. The tenacity, elongation, and initial modulus ($T/E/M$) are, respectively, in the range of 9.5–10.7 g d^{-1}, 6–9%, and 130–150 g d^{-1}. Experimental filaments also exhibit excellent resistance to yielding within the range of small strain, with tensile stress values as high as 5–7 g d^{-1} being observed at 5% elongation. This superior balance of properties, high modulus, high tenacity and high dimensional stability, is unprecedented in conventional commercial processes for the production of PET filament.

(Keywords: poly(ethylene terephthalate); high performance fibre; threadline modification)

INTRODUCTION

Continued improvement in the mechanical properties of PET filament yarns has been an ongoing quest for many scientists and engineers. Thus far, most industrial approaches toward this goal have been centred around modifications and/or enhancements to the existing spin–draw technology. In this traditional two-step process, as-spun fibres of low orientation, and low crystallinity are initially formed, and then subjected to an integrated drawing and heat-setting process to obtain the final product. The mechanical properties of such products, however, appear to have reached their limit. Typically, birefringences of these commercial filament yarns are on the order of 0.20–0.22, with tenacity, elongation, and initial modulus values reaching around 8–9 grammes per dernier (gd^{-1}), 10–15%, and 80–100 gd^{-1}, respectively. Since these values fall well below predicted theoretical limits, the search for improved processing techniques is still considered an important and urgent task, for both industry and academia.

In our continuing research, we have found that the structural features and mechanical properties of the as-spun filaments produced from a melt spinning process can be significantly influenced and/or controlled with the introduction of a liquid isothermal bath (LIB) in the spinline[1–4]. The as-spun fibres prepared under optimum LIB operating conditions exhibit unique structural features. When the LIB is located distant enough from the point of extrusion, such that the threadline velocity has reached a significantly high value, the drag experienced by the threadline as it passes through the bath results in the development of an extremely high threadline stress. This high threadline stress is believed to stretch, and make more taut, the constituent molecular chains. It has also been hypothesized, that this maintained straining of the molecular chains may render them less mobile, and thus lead to a restriction of the crystal growth process. The present experimental results of LIB as-spun filaments produced at high speeds which possess low crystallinity and high amorphous orientation are believed to substantiate our hypothesis. The mechanical properties of these LIB as-spun filaments are comparable to those of commercial products from two-step processes, with initial modulus, tensile strength and breaking elongation of *ca.* 100–120 gd^{-1}, 8–9 gd^{-1} and 15%, respectively.

Since the structure of precursor or as-spun filament has a major impact on the properties of the subsequent drawn and heat-set final product, an obvious question arises. What level of mechanical properties might be achieved if these unique LIB as-spun filaments are

*To whom correspondence should be addressed. Present address: College of Material Science and Engineering, Beijing University of Chemical Technology, Beijing 100029, China

Table 1 Preparation conditions of various fibre samples

Sample	Remarks	Spinning		Heat setting		Hot drawing		Denier
		Take-up velocity ($m\,min^{-1}$)	LIB temp. (°C)	Temp. (°C)	Time (min)	Temp. (°C)	Draw ratio	
A	LIB as-spun fibre ($IV = 0.60\,dl\,g^{-1}$)	5000	150	–	–	–	–	5.06
B	Hot drawing from A	–			–	180–200	1.17	4.34
C	LIB as-spun fibre ($IV = 0.97\,dl\,g^{-1}$)	4500	160	–	–	–	–	4.93
D	Hot drawing from C	–	–		–	180–200	1.16	4.24
E	Conventional tire yarn	–		–	–	–		5.34
F	HMLS tire yarn	–			–	–	–	2.77
G	Heat set from A		–	180	5		–	5.11

subjected to drawing and heat-setting? In a previous publication, it was suggested that some of the unique features of the LIB as-spun filaments may act to accelerate structure development during post-treatment[4]. In this study, the LIB was used to modify the structure of the as-spun filament; these filaments were then slightly drawn and heat-set. The structural features and mechanical properties of both the as-spun and drawn/heat-set filaments from an LIB spinning process were then compared to both a conventional and high modulus low shrinkage (HMLS) commercial yarn.

EXPERIMENTAL

Preparation of samples

Two types of PET chips with intrinsic viscosities (IV) of $0.97\,dl\,g^{-1}$ and $0.60\,dl\,g^{-1}$, as measured in a 60/40 wt% phenol/tetrachloroethane solvent at 25°C, were utilized in this study.

Sample designations and the preparation conditions are given in *Table 1*. Samples A and C are as-spun filaments produced using the LIB spinning process, with low and high molecular weight chips, respectively. A detailed description of the LIB modified melt spinning process has been provided in a preceding publication[3]. Sample A was produced at a take-up velocity of $5000\,m\,min^{-1}$, with the bottom of the bath located 100 cm from the spinneret (LIB position 2), and the liquid depth and temperature fixed at 20 cm and 150°C, respectively. Sample C was produced at a take-up velocity of $4500\,m\,min^{-1}$, with the bottom of the bath located 180 cm from the spinneret (LIB position 3), and the liquid depth and temperature fixed at 30 cm and 160°C, respectively. Both of these as-spun filaments (A and C) were subsequently hot-drawn at 180–200°C using a feed rate of $10\,m\,min^{-1}$ with an imposed draw-ratio of 1.16–1.17. This draw-ratio was arrived at by first experimentally determining the maximum possible and then reducing it just enough to allow for continuous filament to be generated. As shown in *Table 1*, the drawn and heat-set filament produced from sample A was designated as sample B, and the drawn and heat-set filament produced from sample C was designated as sample D. Two commercial PET yarn samples (E and F) produced through traditional two-step processes are also listed in *Table 1*. While the details regarding the production of these commercial samples are not available, a clearly distinguishable feature is observed when the mechanical properties and shrinkage characteristics of these two samples are compared. The conventional yarn has a high tenacity, but also has a characteristic, and undesirable, high shrinkage. Whereas, the HMLS yarn has a low shrinkage, but also has a characteristically, and undesirable, low tenacity. These two samples were obtained as multifilament yarns and then separated into single filaments for study. Their structural features and mechanical properties will be discussed in greater detail during later comparisons with the LIB spun filaments. Sample G is another post-treatment product generated from as-spun sample A. In this case, the as-spun filament of sample A was heat-set under a constant length condition in a 1,2-propanediol circulated bath maintained at 180°C for 5 min. The chosen heat setting temperature of 180°C has been reported to be close to the temperature at which the crystallization rate is the highest in PET[5].

Characterization techniques

Birefringence measurements were performed using a Leitz 20-order tilting compensator mounted in a Nikon polarizing microscope. The volume fraction crystallinity was calculated from density values measured in a sodium bromide density gradient column, as described in the preceding paper[2].

Fibre denier was determined by the vibroscope method in accordance with ASTM D1577. The linear density of the sample was calculated based on the following equation:

$$\text{linear density (in units of g m}^{-1}) = t/(4L^2f^2)$$

Here t is the pretension applied on the fibre, L is the effective fibre length, and f is the fundamental resonant frequency.

Wide angle X-ray scattering (WAXS) patterns were photographed with a vacuum flat camera using a Siemens type-F diffractometer system. A copper target in conjunction with a nickel filtered CuK_α radiation source was used for all the X-ray photography. The WAXS intensity curves for equatorial, meridional, and azimuthal scans were measured using the same system. Resolution of overlapping diffraction peaks was performed with a commercially available profile curve fitting program 'PeakFit™'. The determination of apparent crystallite dimensions and the crystalline and amorphous orientation factors (f_c, f_a) was accomplished using traditional methods as described previously[2].

Small angle X-ray scattering (SAXS) patterns were also obtained using the same photographic system. A

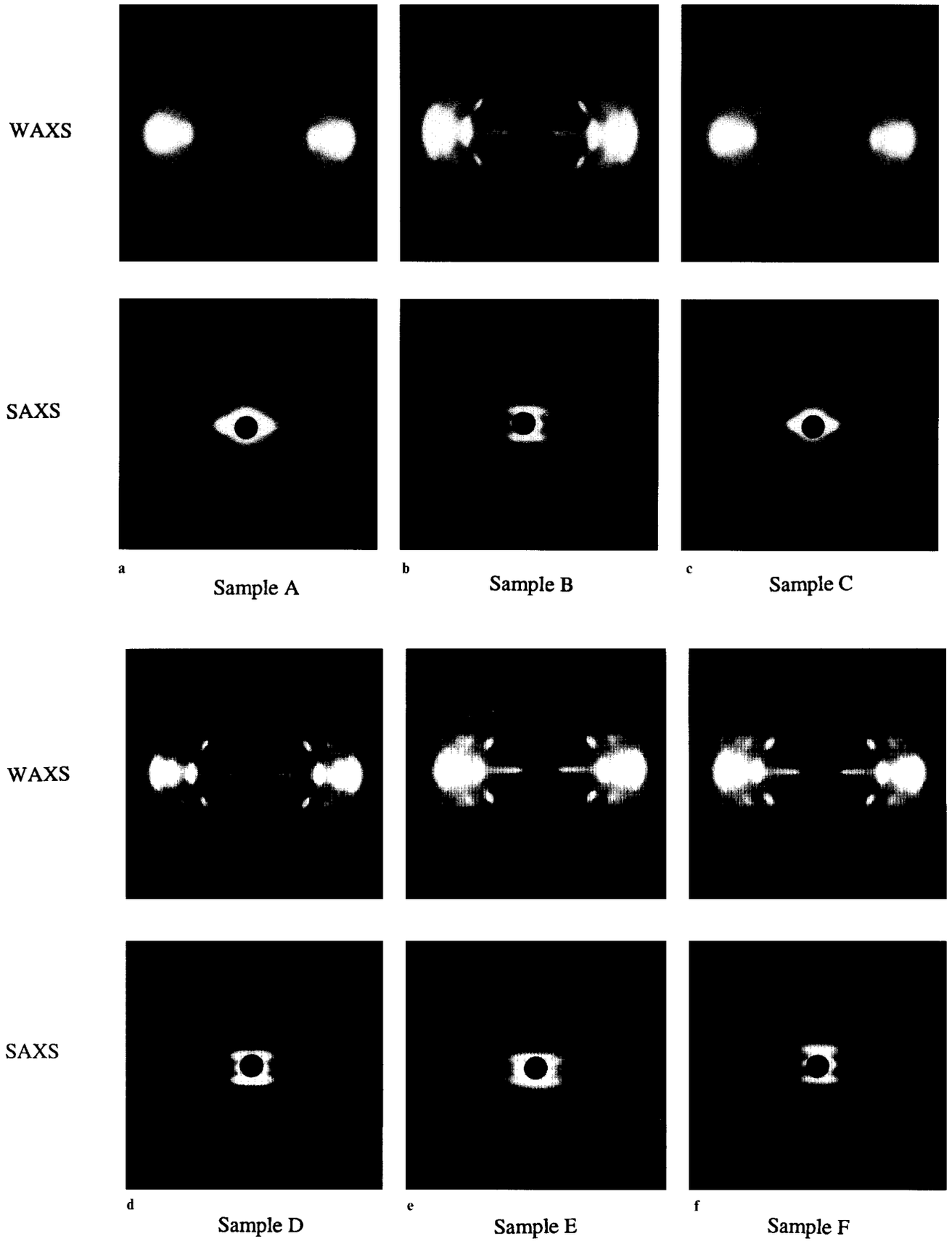

Figure 1 WAXS (top) and SAXS (bottom) patterns of six different PET fibre samples

fibre sample holder with a pinhole collimator of 0.25 mm diameter and a sample–film distance of 30.5 cm were used. The long period spacing (LPS) was calculated from a measurement of the separation of meridional streaks in a direction parallel to the fibre axis by application of the Polanyi equation[6]

$$n\lambda = l * \sin \Phi$$

where n is unity for first-order layer lines, l is the long period spacing, and Φ is half of the angular separation of meridional streaks.

The structural characteristics of the fibres were also examined by unpolarized infra-red (i.r.) spectroscopy. The i.r. absorption spectra were recorded with a Nicolet 510P spectrophotometer. Sample preparation and the fitting of absorbance bands corresponding to particular molecular vibrations followed the method described in ref. 3.

Tensile testing was performed on an Instron machine model 1122. Single filaments were tested using a gauge length of 25.4 mm and a constant crosshead speed of 20 mm min^{-1}. This Instron tensile tester was also used for hysteresis measurements. The fibre samples with lengths of 25.4 mm were stretched to 5.0% extension and retracted. In order to obtain reliable initial moduli, a large magnification was applied to the extension axis. The crosshead speed was chosen to be 5 mm min^{-1}, and the chart speed was chosen to be 500 mm min^{-1}. The cycling was repeated 50 times. The stress–strain curves of the first and 50th extension cycles were recorded. From these hysteresis curves, load at specified elongation of 5% (LASE-5), energy lost during cyclical straining, and permanent strain after 5% elongation were calculated.

Shrinkage was calculated as the percentage change in length when the fibre was exposed to hot air at 177°C, in accordance with ASTM D885.

RESULTS AND DISCUSSION

Structural properties of experimental and commercial filament samples

WAXS patterns of filament samples A and C are shown in *Figures 1a* and *1c*, respectively. Comparison of these patterns indicates the presence of similar structural features. No uniform amorphous halo is observed in either of these samples. In fact, both reflections present tend to concentrate towards the equator with the arcs becoming relatively narrow. While these reflections are weak and indicative of small or poorly developed crystals, the concomitant narrowing of the arcs supports the existence of a high degree of chain alignment along the fibre axis. Note, these crystallite reflections do not appear similar to those of a filament produced from an unperturbed high-speed spinning process, or a commercially produced spin–draw yarn. For example, the diffraction pattern of a filament spun at a take-up velocity of 5000 m min^{-1} without threadline modification (unperturbed) typically shows both a more highly developed crystalline structure and high crystal orientation[7,8]. As previously hypothesized, the poor crystalline development observed in the LIB as-spun filaments is believed to be a result of the extremely high tension imposed by the presence of the liquid bath in the spinline[1,3]. Such a significant increase in the threadline tension may limit segmental motion of the molecular chains and reduce crystalline growth, while maintaining extended molecular chains in the amorphous phase. This results in decreased crystallite size, low crystallinity, and a high amorphous orientation, as shown in *Table 2*.

Figures 1a and *1c* also show the SAXS patterns of the same two samples described above. It is seen that threadline modification does not lead to the appearance of a SAXS maximum in the meridional direction. This may be related to the low scattering capability of these samples, due to their low crystallinity. Another possible explanation for the absence of scattering streaks in the meridional direction may be that only a small density difference exists between the crystalline and amorphous phases[9]. The as-spun fibres prepared using the LIB are characterized by extremely high amorphous orientation, this increase in orientation being most likely accompanied by an increase in the amorphous phase density. An equation relating amorphous orientation and amorphous density, in which amorphous density increases linearly with increasing orientation, has been proposed previously[10,11]. Assuming the density of the crystalline phase is constant, an increase in the amorphous phase density would thereby result in a smaller density contrast between the two phases and the absence of a meridional streak, even if some level of regular longitudinal periodicity were present. As described above, this contrast reduction may be the reason for the weak, or non-existent, meridional scattering peaks associated with the presence, or lack thereof, of a long period spacing.

Samples A and C were subsequently hot-drawn, the resulting samples were labelled B and D, respectively. Even though the draw ratios were extremely low, 1.16–1.17, and the heat treatment times short, 6.0–7.0 s, considerable structural changes occurred in both cases. The WAXS diffraction patterns of samples B and D are also shown in *Figure 1*. The diffraction patterns of B and D indicate a highly preferred orientation of the crystalline chains parallel to the drawing direction. The much more perfect crystalline structure of these samples is evidenced by their sharp and resolved diffraction spots, which is considered to be an essential distinction when compared with their as-spun precursors A and C. Further, the crystal structure of samples B and D resembles closely that of commercial samples E and F, whose

Table 2 Structural analysis of various fibre samples

Sample	Crystallite dimensions (nm)				x_v (%)	Δn	fc	fa	LPS (nm)
	$\bar{1}05$	010	$\bar{1}10$	100					
A	3.35	2.71	2.17	1.80	20.0	0.222	0.936	0.822	–
B	4.87	4.58	4.29	2.90	53.8	0.235	0.979	0.938	15.4
C	3.06	2.74	2.00	1.98	15.2	0.214	0.940	0.783	–
D	4.76	4.86	3.92	2.96	50.2	0.237	0.973	0.946	16.2
E	3.85	4.50	3.39	2.80	48.6	0.215	0.969	0.788	17.4
F	3.78	4.28	4.14	2.76	47.5	0.202	0.951	0.713	13.1
G	4.48	4.06	3.42	2.78	42.6	0.224	0.942	0.860	13.4

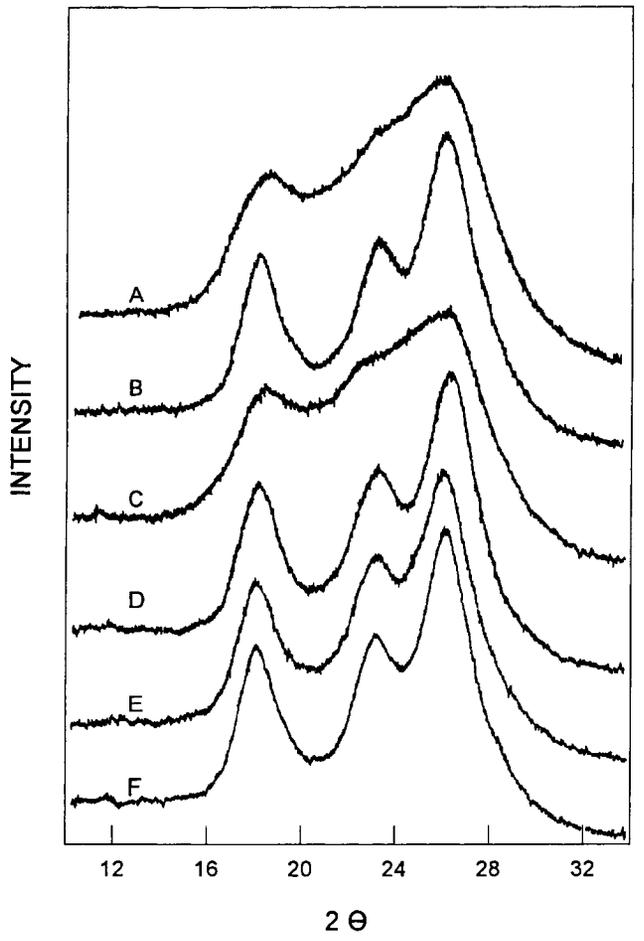

Figure 2 Equatorial X-ray diffraction profiles of fibre samples A–F

diffraction patterns are also shown in *Figure 1*. *Figure 2* shows the corresponding WAXS equatorial diffraction scans of the same six samples shown in *Figure 1*. These equatorial scans show in greater detail the same structural features eluded to from observation of the diffraction patterns presented in *Figure 1*. The poorly resolved scans of samples A and C were transformed to the well resolved scans of samples B and D, respectively. The individual diffraction peaks (010, $\bar{1}10$, 100) are clearly present in the two hot-drawn LIB samples (B and D), as well as, in the two commercial samples (E and F), indicating that crystal growth was well developed in each of these samples. Measurements of the half-widths of WAXS equatorial and meridional diffraction peaks permitted an estimation of the apparent crystallite sizes from the Scherrer equation[12]. The results of these measurements are presented in *Table 2*. For those samples which showed distinguishable meridional streaks in the SAXS photographs, samples B, D, E and F, the long period spacing was also calculated, these results are also presented in *Table 2*.

In addition to the crystallite sizes (L_{010}, $L_{\bar{1}10}$, L_{100} and $L_{\bar{1}05}$) and long period spacings (LPS), *Table 2* also presents the results from further structural analysis which included the measurement of crystallinity ($Xv\%$), birefringence (Δn), and crystalline and amorphous orientation factors (f_c and f_a) for samples A through G. As shown in *Table 2*, after the hot drawing was performed on the LIB as-spun fibres, the apparent crystallite sizes, and overall crystallinity increased significantly. Birefringence, f_c and f_a also increased, but to a lesser degree. The crystallite sizes and crystallinities of the hot drawn filaments (B and D) are *ca* 1.5–2 and 2–3 times higher than that of the LIB as-spun filaments (A and C), respectively. The crystallite sizes, crystallinity and long period spacing of the two hot drawn filaments (B and D) are quite similar to each other, as well as, to those of the two commercial samples (E and F), indicating that a similar crystalline structure exists among these four samples. However, it must be noted that molecular orientation, especially the birefringence values and amorphous orientation factors, show some small but important differences among the six samples. Both LIB as-spun filaments A and C have a high birefringence on the order of 0.22, and high amorphous orientation, *ca* 0.8–0.9. These respective values are equal to, or greater than, those of the conventional tire yarn, and is presented as the main reason for the fact that the LIB as-spun filaments have mechanical properties approaching those of the commercial yarns produced via the traditional two-step spin–draw process (see *Table 4*).

When this LIB as-spun filament (A and C) was subjected to hot-drawing, further increases in the birefringence ($\Delta n > 0.235$) and in both the crystalline and amorphous orientation factors were achieved. One reference taken from the literature, on the structure and mechanical properties of zone-annealed PET, cites the attainment of a birefringence value of 0.247[13]. Such super high molecular orientation, however, was attained using an extremely low drawing speed, and numerous repetitions of the zone drawing and annealing. It is not unusual to expect that high drawing under high temperature, maintained for extended periods of time, would induce the formation of a more perfect crystalline structure, where an obvious increase in crystallinity and crystallite dimensions would result. However, as previously stated, in this study the maximum draw ratio capable of being achieved in both the low and high molecular weight as-spun fibres was only 1.16–1.17, and the heat-treatment time only approximately 6–7 s. It is surprising that such significant structural changes occurred, even though the hot-drawing process was so limited. In order to understand this phenomenon more clearly, a second sample was prepared from the original as-spun sample A, this sample was subjected to a constant length heat-setting process at 180°C for 5 min and is labelled sample G. *Figure 3* shows both the WAXS and SAXS photographs of Sample G. Comparing the results from X-ray analysis of samples A, B and G, it is clear that the crystalline structure of sample G is quite different from sample A, but appears similar to sample B with respect to the crystallite size, overall crystallinity and crystalline orientation (see *Table 2*). These experimental data indicate that the crystalline structure of sample G has been fully developed, simply through heat setting. One plausible explanation for such behaviour may reside in the supposition that a high proportion of semi-ordered structure, or alternately, a highly oriented amorphous phase exists in the as-spun fibre. Within this phase, highly stretched, very taut molecular chains have been formed as a result of the extremely high tension developed in the threadline by the high fractional drag developed within the LIB. When such samples were subjected to either hot-drawing or heat-setting, the occurrence of large-scale molecular shifts may be

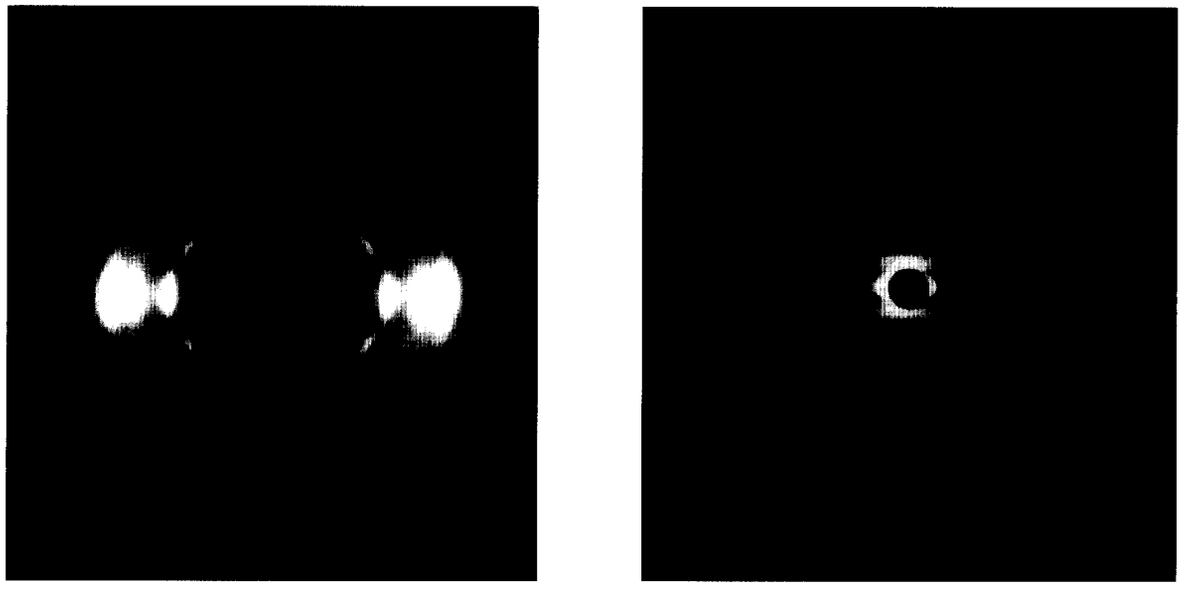

Figure 3 WAXS (a) and SAXS (b) patterns of sample G

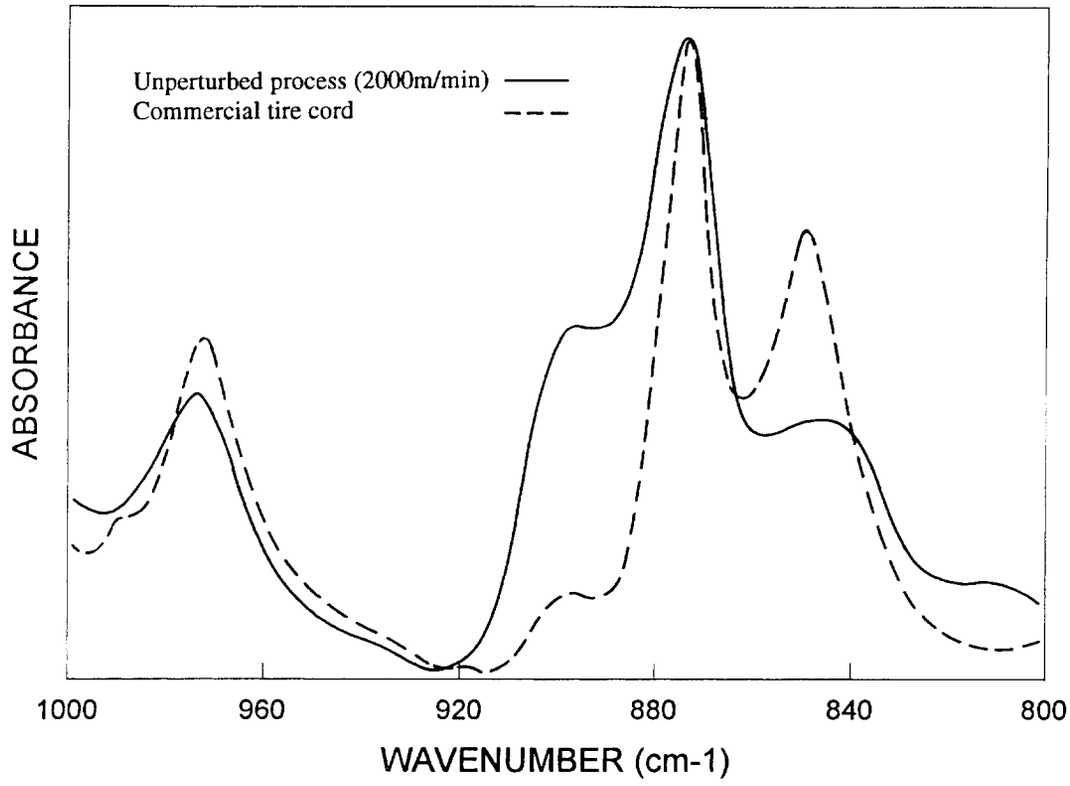

Figure 4 Unpolarized i.r. spectra of sample E and an unperturbed melt spun (take-up velocity = 2000 m min^{-1}) fibre in the wavenumber region of 800–1000 cm^{-1}

disregarded because the draw ratio was zero or extremely small. Instead, high temperature could have activated local thermal motions and allowed the highly stretched, very taut amorphous chains (one-dimensional ordered phase) to be converted into a near perfect crystalline phase (three-dimensional ordered phase). The result being a significant transformation from highly oriented amorphous chains to a highly oriented crystalline phase.

I.r. spectroscopy was also used to analyse and interpret the data. The following absorbance band assignments are presented in accord with refs 14–16. The absorbance bands at 848 and 972 cm^{-1} have been assigned to the combined crystalline and amorphous *trans* conformers. The absorbance band at 899 cm^{-1} has been assigned to the *gauche* conformers, which are taken to be present only in the amorphous phase. The typically small and overlapping absorbance band at 988 cm^{-1} has been assigned to the fold content at the surface of crystals[15]. The absorbance band at 875 cm^{-1} is associated with vibrations of the benzene ring and is not directly affected

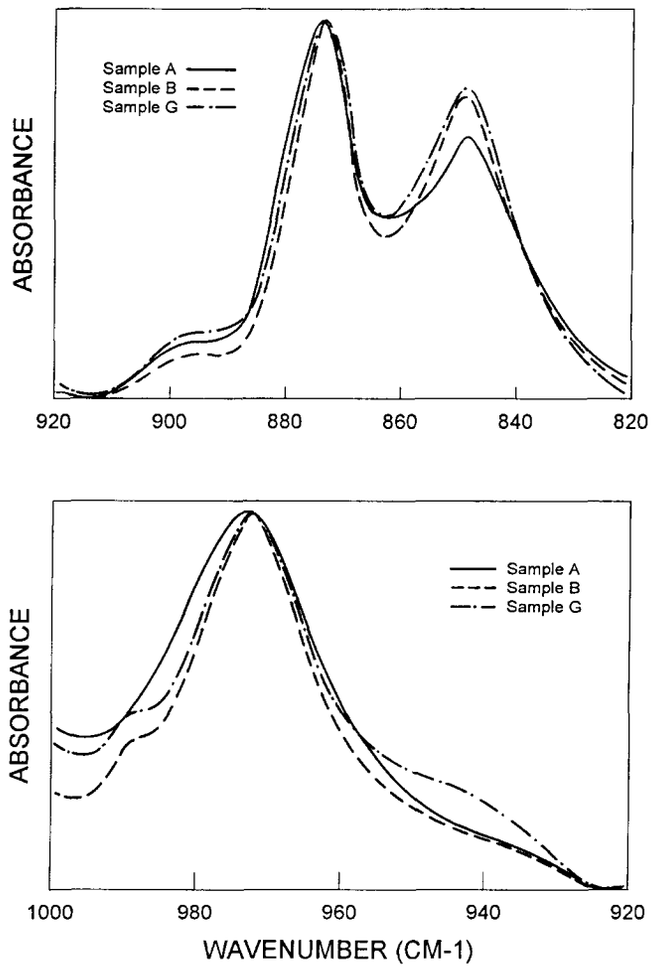

Figure 5 Unpolarized i.r. spectra of the samples A, B and G in the different wavenumber regions 820–920 cm^{-1} and 920–1000 cm^{-1}

Table 3 Dependence of absorbance ratio and band halfwidth on the sample preparation condition

	Absorbance ratio			Halfwidth (cm^{-1})	
Sample	A_{972}/A_{872}	A_{848}/A_{872}	A_{899}/A_{872}	972 cm^{-1}	848 cm^{-1}
UM2000	0.288	0.374	0.501	18.2	23.1
E	0.509	0.828	0.079	17.3	18.7
A	0.553	1.063	0.153	20.3	22.0
B	0.695	1.371	0.135	16.9	19.3
G	0.675	1.178	0.145	16.9	20.1

by conformational changes, hence its magnitude was used as an internal standard to normalize between samples for variations in mass. This allows for direct quantitative comparisons between samples regarding the relative amounts of each conformer type present. The relative intensity of such conformation-sensitive bands have been frequently used for the evaluation of morphological changes[13,16,17]. Generally, when the dominant molecular conformation within a PET filament changes from a random coil status to a stretched or straighter chain morphology, the relative intensities of the *trans* bands are increased, while the *gauche* band is decreased.

The unpolarized i.r. spectra of two filaments, one produced by the unperturbed process at a take-up velocity of 200 m min^{-1} (sample UM2000) and sample E are shown in *Figure 4*. In this case, the structure of the unperturbed as-spun filament produced at 2000 m min^{-1} is considered to be representative of a conventional tire yarn prior to drawing and heat-setting, with sample E being representative of the final product, after drawing and heat-setting. Generally, the as-spun precursor filament of this type has low crystallinity and low molecular orientation, while the drawn and heat-set filament possesses a high crystallinity and high molecular orientation. The changes in relative intensity of the 848 and 899 cm^{-1} bands, as observed in *Figure 4*, show clearly that significant structural changes occur during the high temperature drawing in a traditional spin-draw process. The high temperature drawing transforms many of the randomly coiled chains into extended chains, resulting in a large percentage of *trans* conformations in the final product. For comparison, the unpolarized spectra of samples A, B and G are shown in *Figure 5*. The lower wavenumber region contains one of the *trans* bands (848 cm^{-1}), the benzene ring reference band (875 cm^{-1}) and the *gauche* band (899 cm^{-1}); the higher wavenumber region contains the second *trans* band (972 cm^{-1}), as well as, the previously described fold band (988 cm^{-1}). As indicated in *Table 2*, the crystallinity in hot-drawn sample B and heat-set sample G is about 2–3 times higher than that of the precursor LIB as-spun sample A. The significant increase of the crystallinity in samples B and G is accompanied by the appearance of a small shoulder, or weak absorbance band, at 988 cm^{-1}. This suggests that at least some portion of the newly developed crystalline structure is made up of folded

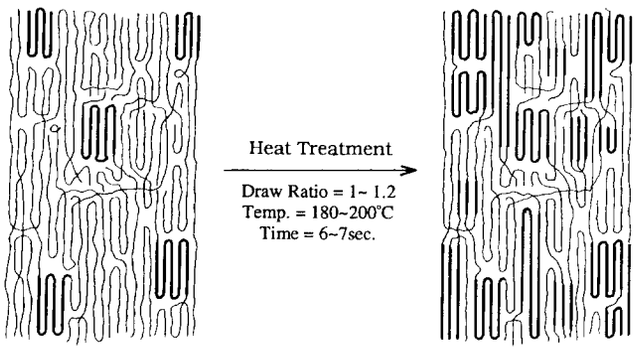

Figure 6 Model illustrating the morphological changes in high amorphous orientation/low crystalline LIB as-spun fibre subjected to the hot-drawing process

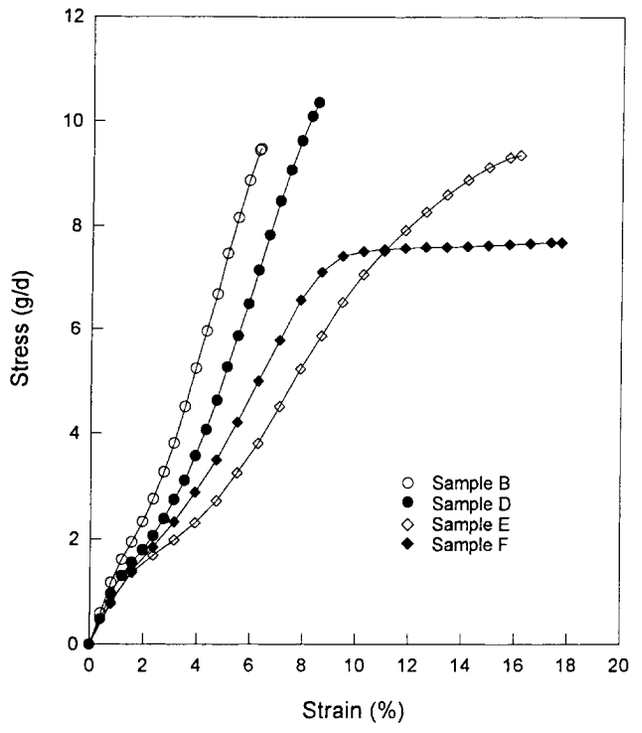

Figure 7 Comparison of the stress–strain behaviour for two experimental samples, B and D, and two commercial samples, E and F

chains. However, after being normalized, the relative intensities of both the *trans* and *gauche* bands do not change significantly during hot-drawing or heat-setting, as shown in *Table 3*. This indicates that the molecular alignment originally present in as-spun LIB sample A was not perturbed to any great extent during the hot-drawing or heat-setting processes, this point is in contrast to the situation observed for the low-speed low orientation precursor filament which is subsequently highly drawn and heat-set. We must also note some of the finer details present in these spectra. For instance, the *trans* absorbance bands at 848 and 972 cm^{-1} are composed of both crystalline and amorphous contributions, in which the contributing crystalline component is represented by a narrow band, while the contributing amorphous component is represented by a relatively wider band[16]. As shown in *Figure 5*, the half-width of both the 848 and 972 cm^{-1} bands become gradually narrower upon either hot-drawing or heat-setting. This corresponds to the transformation of extended chain amorphous material into the crystalline phase. The small draw ratio, or fixed length condition, imposed during the production of samples B and G suggests that only small local motions or rearrangements could have occurred during the transformation from the amorphous to the crystalline phase. Therefore, the highly oriented extended chain amorphous material which crystallized, may have resulted in the formation of some small fraction of an extended chain crystalline phase. This presumption stemmed from an attempt to justify the extremely high measured modulus values of samples B and G. While insufficient evidence is presented here to unequivocably conclude the existence of this extended chain crystalline phase, a possible model structure depicting its development has been proposed. As shown in *Figure 6*, the as-spun LIB filament possesses a large percentage of extended chains in the amorphous regions, which upon hot-drawing are believed to result in greater connectivity among neighbouring crystallites, as well as, fewer folds being present at the surface of the crystalline material formed during the hot-drawing process. Future research efforts will attempt to further clarify the appropriate type of model for both as-spun and hot-drawn filaments produced using this LIB technology.

Mechanical properties of experimental and commercial filament samples

Figure 7 shows the stress–strain curves for the four samples B, D, E and F. The tenacity, breaking elongation and initial modulus derived from these curves are summarized in *Table 4*, together with representative shrinkage data. In general, the curves shown in *Figure 7* reveal a yield point in the vicinity of the origin. The elongation occurring in the region from the origin to the yield point, is considered to be elastic extension. The slope of the initial straight portion represents the initial modulus, or the amount of work required to move molecular segments from their equilibrium positions. Beyond the yield point, large-scale molecular motion may begin with molecular uncoiling or rotation associated with the *gauche–trans* transition occurring[18], leading to little change of the stress as deformation continues. With further elongation, a so-called strain-hardening phenomenon occurs, due to the concerted, continuous extension of the molecular chains, in this region. Outside of this region, fibre breakage or large viscoelastic movement can occur. As shown in *Figure 7*, the conventional tire yarn (sample E) possesses a typical stress–strain curve. It displays a high tenacity with modest modulus and breaking elongation. Sample F has a slightly higher modulus than that of sample E, but exhibits an obvious second yield point, where the stress reaches a plateau region as the elongation increases. As a result, it has the lowest tenacity and largest breaking elongation. Another feature common to both samples E and F is that the yield points in their respective stress–strain curves are responsible for the relatively low value of the LASE-5. Unlike the two commercial samples, fibres produced by the combination of our threadline modification and post-drawing process have excellent mechanical properties. As expected from their structural features, samples B and D displayed both a high modulus and high tenacity. Their tenacities are as high as, or greater than, that of the conventional tire yarn (sample E). In the case of sample D, the tenacity reaches 10.3 gd^{-1}. More importantly, the

Table 4 Mechanical properties of various fibre samples

Sample	Tenacity (gd^{-1})	Modulus (gd^{-1})	Elongation (%)	Shrinkage (%)	Energy lost (erg)		Energy lost/energy input (%)		LASE-5 (gd^{-1})	Permanent strain (%)
					1st	50th	1st	50th		
A	7.98	124	8.3	11.5	–	–	–	–	4.86	–
B	9.50	146	6.3	3.8	1.06	0.59	24.6	15.9	7.28	0
C	8.80	129	8.9	13.8	–	–	–	–	5.00	–
D	10.3	128	9.1	3.8	0.94	0.54	31.8	21.0	5.10	6.2
E	9.50	96	16.6	13.7	1.12	0.33	53.6	27.4	3.08	27.6
F	7.40	88	16.5	5.9	0.90	0.36	35.6	19.5	3.79	9.2
G	7.63	132	8.4	4.3	–	–	–	–	5.31	–

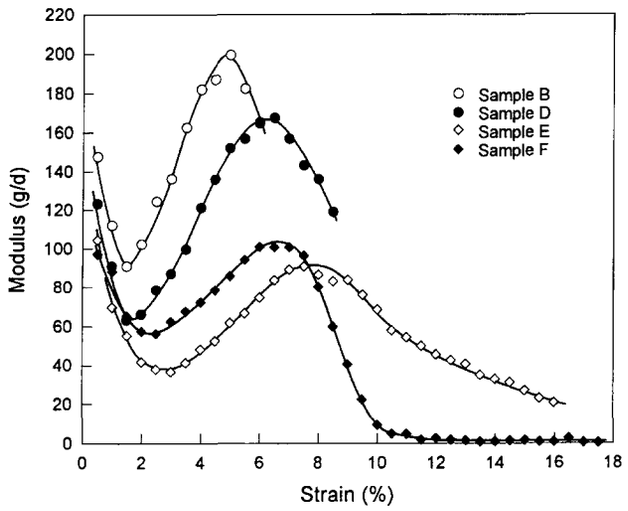

Figure 8 Comparison of the modulus–strain curves for experimental samples B and D, and commercial samples E and F

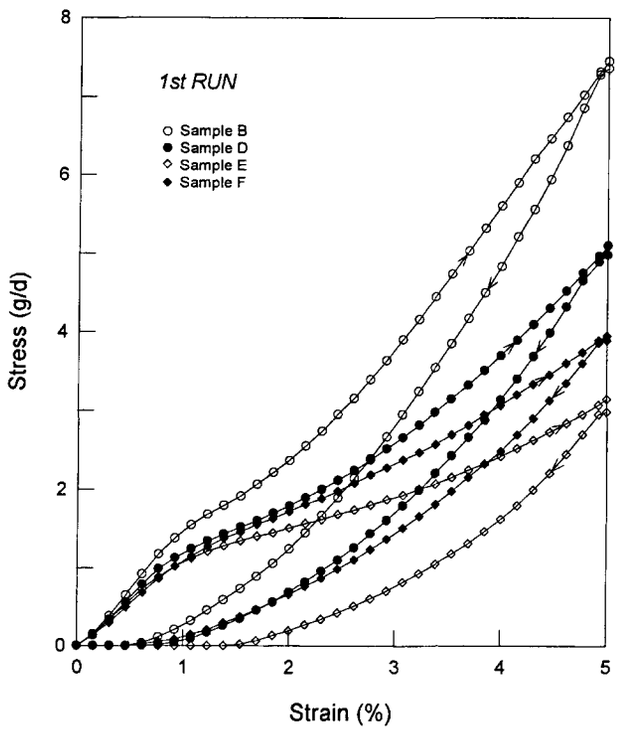

Figure 9 Comparison of the first running hysteresis curves for experimental samples B and D, and commercial samples E and F. The arrows indicate the direction of crosshead travel

initial modulus in these two experimental samples, especially in sample B, are also improved significantly. The modulus of these samples reached 130–150 gd^{-1}. As shown in *Figure 8*, the experimental samples always exhibit a higher modulus than that of either of the commercial yarns over the entire range of strain. It is also worth noting that the yield points in the stress–strain curves of the experimental samples are not so distinct as observed in the curves of the commercial yarns. In other words, the slope of the curve beyond the yield point does not decrease dramatically. This could be attributed to some unique structural feature of the experimental samples. The high crystallinity and the presumed higher fraction of tautly extended amorphous chains would make molecular uncoiling or rotation more difficult. This results in samples B and D possessing extremely high LASE-5 values of 7.3 and 5.0 gd^{-1}, respectively. These LASE-5 values are about two times higher than those of the filaments taken from the commercial yarns.

Furthermore, as shown in *Table 4*, samples B and D exhibit a slight, but significant difference between their mechanical properties. Sample B made from the low molecular weight PET chip, possesses a slightly lower tenacity, but higher modulus and LASE-5. The above difference in these particular properties between the low and high molecular weight samples was considered to be related to the variation in crystallinity. The chains present in the low molecular weight material are believed to be somewhat more mobile and capable of allowing for the development of a greater percentage of crystalline material. As the amount of crystallinity increases the connectivity of the structure increases, as well as, the initial resistance to straining. The higher tenacity of the high molecular weight material is a typically observed phenomenon, and is presumed to be a result of the increase in average length of overlapping chain segments.

To examine the extension cycling behaviour, which is a combination of the effects of elastics recovery, viscoelasticity, and fatigue, the loading history of samples B, D, E, and F was studied. The fibres were stretched to 5.0% elongation and allowed to retract at room temperature. This operation was repeated 50 times. The results of the first and the 50th run were recorded and are shown in *Figures 9* and *10*, respectively. As shown in *Figure 9*, there is a gradual increase of the maximum stress at 5.0% elongation for the four samples. As indicated in both *Figure 9* and *Table 4*, sample B had the highest LASE-5 (7.3 gd^{-1}) among the four samples, followed by sample D (5.0 gd^{-1}), then sample F (3.3 gd^{-1}), and the lowest for sample E (2.9 gd^{-1}). Also note, experimental samples B and D both possess a higher initial modulus than the filaments taken from either of the commercial yarns. As

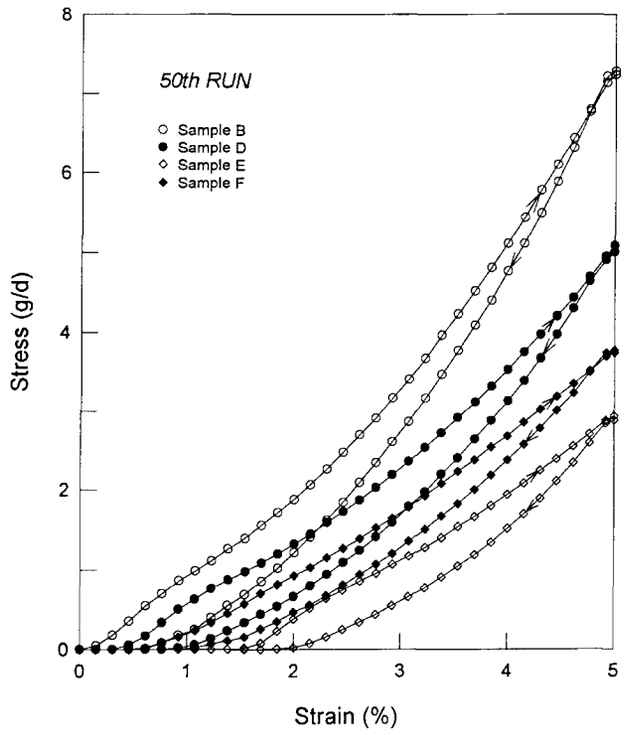

Figure 10 Comparison of the 50th running hysteresis curves for experimental samples B and D, and commercial samples E and F. The arrows indicate the direction of crosshead travel

listed in *Table 4*, the hysteresis (the fraction of the energy lost during cyclical straining) calculated from the area enclosed by the extension and retraction curves, differs little for the four samples. However, the ratio of the energy lost to the input strain energy during a cycle is significantly lower in the two experimental fibres, especially in sample B. In both the first and the 50th run, the respective values of this ratio for sample B are only 25% and 16%, compared with values of 53% and 27% for the conventional tire yarn (sample E). This fact demonstrates that the experimental filament samples B and D have greatly improved elastic recovery, and diminished viscous creep. Such a conclusion is also supported by the observation that the permanent strain, which was calculated by dividing the residual strain present in each of the 50th run extension curves by the imposed strain of 5%, is also lower in the experimental samples B and D. It is surprising that after 49 repetitions of the extension cycle, experimental samples B and D exhibit such an extremely small permanent strain. This excellent elastic recovery behaviour is attributed to the high molecular orientation and high crystallinity achieved in the experimental samples produced using the combination of an LIB modified high-speed spinning process and traditional post-treatment methods.

CONCLUSIONS

A process for producing high modulus, high strength, dimensional stable PET filament by combination of threadline modification and post-drawing techniques was investigated. The imposed threadline modification was the placement of a LIB along some portion of the melt-spinning threadline. Greater detail regarding this particular bath and its operation has been discussed in a previous publication[3]. The presence of the bath has forced the development of very high threadline tensions[1,2]. The as-spun LIB filaments were found to possess a low level of crystallinity and a high level of overall orientation. The high level of orientation was considered to be a direct result of the high threadline tension experienced during the production of these filaments. The low level of crystallinity, however, seemed at first to contradict the notion that rates of crystallization in a melt-spinning threadline increase as the orientation of the constituent molecules increase. It has been hypothesized that the high threadline tension acts to limit chain segment mobility, which in turn restricts that rate of crystallization[1]. Even though high axial orientation may be present, some small dispositions of the chain segments would be required in order to accommodate the continued growth of such a perfectly ordered structure as a crystallite. It has also been hypothesized that the unique as-spun structure which results from this LIB modified spinning process may also lead to accelerated structure development when the filament is subjected to traditional post treatment, such as a hot-drawing or heat-setting process. The results from these post treatment studies do indeed indicate that near fully developed structures, comparable to commercial PET industrial yarns, can be produced with the use of relatively small draw ratios and minor heat treatments. In fact, the combination of threadline modification and minor post treatment has allowed for the production of PET filaments which possess mechanical properties superior to those of commercially produced industrial yarns, in which a relatively low orientation as-spun feedstock yarn is subjected to more severe drawing conditions. The findings presented in this study further demonstrate the radical control over both as-spun and post-treated PET filament structure and mechanical properties which can be achieved through appropriate modification to the dynamics of a melt-spinning threadline.

REFERENCES

1 Cuculo, J. A., Tucker, P. A. and Chen, G. Y. *J. Appl. Polym. Sci., Appl. Polym. Symp.* 1991, **47,** 223
2 Lin, C. Y., Tucker, P. A. and Cuculo, J. A. *J. Appl. Polym. Sci.* 1992, **46,** 531
3 Wu, G., Zhou, Q., Chen, J. Y., Hotter, J. F., Tucker, P. A. and Cuculo, J. A. *J. Appl. Polym. Sci.*, 1995, **55,** 1275
4 Zhou, Q., Wu, G., Tucker, P. A. and Cuculo, J. A. *J. Polym. Sci., Polym. Phys. Edn* 1995, **33,** 909
5 Alfonso, G. C., Verdona, M. P. and Waslak, A. *Polymer* 1978, **19,** 711
6 Wang, J. I. and Harrison, I. R. 'Methods of Experimental Physics' (Ed. R. A. Fava), Academic, New York, 1980, Chap. 6
7 Ihm, D. W. and Cuculo, J. A. *J. Macromol. Sci.-Rev., Macromol. Chem. Phys.* 1984, **C24,** 419
8 Yasuda, H. 'High-Speed Fiber Spinning' (Eds A. Ziabicki and H. Kawai), Wiley, New York, 1985, Chap. 13
9 Tanigami, T. and Miyasaka, K. *J. Polym. Sci., Polym. Phys. Edn* 1981, **19,** 1865
10 Nobbs, J. H., Bower, D. I. and Ward, I. M. *Polymer* 1976, **17,** 25
11 Huisman, R. and Heuvel, H. M. *J. Appl. Polym. Sci.* 1978, **22,** 943
12 Rim, P. B. *J. Macromol. Sci. Phys. Edn* 1987, **B26,** 19
13 Kunugi, T., Suzuki, A. and Hashimoto, M. *J. Appl. Polym. Sci.* 1981, **26,** 1951
14 Cunningham, A., Ward, I. M., Willis, H. A. and Zichy, V. *Polymer* 1974, **15,** 749
15 D'esposito, L. and Koenig, J. L. *J. Polym. Sci., Polym. Phys. Edn* 1976, **14,** 1731
16 Heuvel, H. M. and Huisman, R. *J. Appl. Polym. Sci.* 1985, **30,** 3069
17 Long, S. D. and Ward, I. M. *J. Appl. Polym. Sci.* 1911, **42,** 1911
18 Heuvel, C. J. M. Van Den, Heuvel, H. M., Feassen, W. A., Veurink, J. and Lucas, L. J. *J. Appl. Polym. Sci.* 1993, **49,** 925